Ergodic Capacity Analysis of Satellite Communication Systems with SAG-FSO/SH-FSO/RF Transmission

Ramy Samy, Hong-Chuan Yang, *Senior Member, IEEE*, Tamer Rakia, and Mohamed-Slim Alouini, *Fellow, IEEE*

***Abstract*—Future non-terrestrial networks aim to achieve a throughput of Terabits/s. Therefore, free-space optical (FSO) communications have been adopted as a candidate solution due to their ability to achieve an extremely high data rate. Nonetheless, FSO communications are sensitive to the adverse effects of beam scintillation, beam-wander-induced pointing errors, free-space loss, and weather conditions. Space-air-ground (SAG) FSO transmission and hybrid single-hop (SH) FSO/radio frequency (RF) transmission are promising solutions to improve the performance of FSO links and can be integrated into a satellite communication (Satcom) system. In this work, we carry out a thorough capacity analysis of the resulting integrated SAG-FSO/SH-FSO/RF Satcom system, where Gamma-Gamma and Rician distributions are used to characterize FSO and RF links, respectively. The exact analytical expressions are derived and validated by Monte-Carlo simulations. We also obtain asymptotic expressions for the ergodic capacity in the high signal-to-noise ratio region. The numerical results highlight the significant potential of the integrated SAG-FSO/SH-FSO/RF Satcom system over existing solutions. We also show that the integrated Satcom system with intensity modulation and direct detection can achieve a capacity gain over that with a heterodyne detection technique over all satellite zenith angles.**

***Index Terms*—Ergodic capacity, Satellite communication, Free-space optics, Space-air-ground networks, Hybrid FSO/RF systems, High-altitude platforms.**

I. Introduction

THE last decade has seen a never-ending growth in mobile data traffic. According to the International Telecommunication Union's (ITU) traffic forecasts, the global mobile data traffic per month is estimated to grow at an annual rate of about 54%, reaching 607 exabytes (EB) in 2025 and 5016 EB in 2030 [1]. In addition to satisfying the demand for ubiquitous coverage, future wireless communication networks are under the burden of efficiently delivering broadband services and connecting numerous Internet of Things (IoT) devices. Terrestrial networks alone are prohibitively expensive to support telecommunication services in hard-to-reach areas of air, sea, and land.

This work was supported in part by the Natural Sciences and Engineering Research Council of Canada (NSERC) Discovery grant.

Ramy Samy and Hong-Chuan Yang are with the Department of Electrical and Computer Engineering, University of Victoria, BC, Canada (e-mail: {ramyzaghloul, hy}@uvic.ca); Tamer Rakia is with the Avionics Department, Military Technical College, Cairo, Egypt (e-mail: tamer_nabiel@mtc.edu.eg); Mohamed-Slim Alouini is with the Computer, Electrical, and Mathematical Science and Engineering (CEMSE) Division, King Abdullah University of Science and Technology (KAUST), Makkah Province, Saudi Arabia (e-mail: slim.alouini@kaust.edu.sa).

To address such challenges, there are ongoing efforts to develop non-terrestrial networks (NTNs) that will achieve cost-effective and high-capacity global connectivity [2]. Augmenting terrestrial communications with aerial networks such as high-altitude platforms (HAPs) is one of the primary solutions. Many projects are being launched, like the Japanese Stratospheric Platform (SPF), European HeliNet and CAPANINA, and Google Loon, with the goal of bringing remote parts of the globe online [3]. Satellite communication (Satcom) systems are another promising solution for future global connectivity. Massive Satcom systems, such as Inmarsat, O3b, Starlink, OneWeb, and Telesat, are being launched into geostationary-earth orbits (GEO), medium-earth orbits (MEO), and low-earth orbits (LEO) to support a wide range of applications with diverse latency requirements. Such Satcom systems represent the next step toward truly ubiquitous communications because of their unique capability of global coverage [4]. Unfortunately, both the above solutions are primarily based on licensed radio frequency (RF) bands with limited capacity and high costs. So, to reduce the cost per transmitted bit to a similar level as terrestrial networks, it is essential to increase the capacity of NTNs to Terabits/s in a cost-effective manner.

In this context, free-space optical (FSO) communications, with their huge available bandwidth, have recently gained an increasing interest in the wireless communication community [5]. But, FSO transmissions are susceptible to beam scintillation, beam wander, pointing errors, and weather conditions such as clouds, fog, and haze [6]. In order to improve the FSO-link performance, an RF link was proposed as a backup [7]. The resulting hybrid single-hop (SH) FSO/RF system explores the complementary properties of FSO and RF links to improve the system reliability [8]. Various diversity schemes, such as maximal ratio combining (MRC) and selection combining (SC), were also proposed for hybrid SH-FSO/RF transmissions [9], [10]. Meanwhile, because of the scarcity of RF spectrum, the RF link can only deliver a data rate of a few Megabits/s. Thus, combining with or switching back to the RF link will reduce the overall system transmission rate. To better explore the Terabits/s transmission rate of FSO links, there is a pressing need to increase FSO-link usability.

Recently, a space-air-ground (SAG) transmission system was proposed in [11], where a HAP relay was deployed between a ground station and a satellite (SAT). The primary objective of such a design is to reduce the effect of pointing error due to beam wandering, which becomes increasingly serious as the propagation distance increases. The introduction

This article has been accepted for publication in IEEE Photonics Journal. This is the author's version which has not been fully edited and
content may change prior to final publication. Citation information: DOI 10.1109/JPHOT.2022.3201046

of a HAP relay effectively divides the single FSO link into two much shorter hops. According to [11], [12], the SAG-FSO transmission achieved a performance gain over traditional SH-FSO transmission in the uplink scenario. On the other hand, it achieves a limited performance improvement over downlink transmission, where the beam-wandering effect is negligible. With the SAG-FSO design in [11], [12], the ground-to-HAP link will experience a similar amount of atmospheric turbulence as direct ground-to-SAT transmission as they share the same zenith angle. While mitigating the beam-wandering effect, the SAG-FSO design in [11], [12] couldn't effectively reduce the atmospheric turbulence experienced by FSO transmission and is more suitable for GEO satellites with a relatively small zenith angle.

To reduce the propagation distance of the optical signal through the strong turbulence region, we can dispatch a HAP with FSO relaying capability directly above the ground station with a very small zenith angle. This proposed SAG-FSO design can effectively reduce the atmospheric turbulence experienced by the ground-to-HAP hop. Note that such a SAG-FSO design will lead to a slightly longer HAP-to-SAT hop, especially when the satellite has a large zenith angle. However, the HAP-to-SAT (HS) link will experience weak turbulence, as the aerosol density is negligible at high altitudes (more than 17 km above the earth's surface) [6]. At the same time, the severity of pointing errors induced by the beam-wandering effect will be substantially reduced. Our SAG-FSO design generalizes the design in [11], [12] for GEO satellites with an arbitrary zenith angle and LEO satellites with varying zenith angles. In order to reap the benefits of FSO's higher transmission rate, such a SAG-FSO transmission with strategically deployed HAP can be combined with conventional hybrid SH-FSO/RF transmission to create a high-throughput and reliable Satcom system as shown in Fig. 1 [13]. Note that, despite the SH-FSO's vulnerability to atmospheric turbulence, it can still support a much higher data rate than RF transmission. Unlike typical hybrid FSO/RF solutions [7]–[12], which use a bandwidth-limited RF link as the only backup for FSO-based Satcom, our proposed system uses SH-FSO link as an additional backup, which can improve system performance and reliability even further. The proposed system will switch to the RF link only when both the SAG-FSO and SH-FSO links are unacceptable.

Previous research examined the performance of hybrid SH-FSO/RF and SAG-FSO/RF Satcom systems in terms of outage probability and average symbol error rate [11]–[14]. However, from the capacity perspective, only a few works have been reported for the hybrid SH-FSO/RF system, and none for the SAG-FSO/RF Satcom systems, to the best of our knowledge. In [8], the authors derived an exact analytical expression for the ergodic capacity of the hybrid SH-FSO/RF system, considering the Gamma-Gamma turbulence channel model for the FSO link and the Nakagami-m distribution with a larger fading severity parameter, m, for the RF link. They also adopted an FSO receiver with intensity modulation and direct detection (IM/DD). In [9], adaptive combining was considered for extra improvement with Gamma-Gamma and $\kappa-\mu$ distributions assumed for FSO and RF links, respectively.

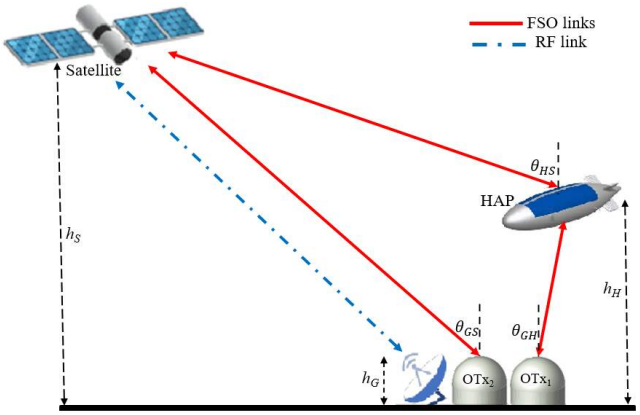

Fig. 1. Satcom system with integrated SAG-FSO/SH-FSO/RF links.

The heterodyne detection (HD) technique was assumed for detecting the FSO signal at the receiver. In [15], the ergodic capacity was analyzed for hybrid SH-FSO/RF, assuming log-normal and Nakagami-m models for FSO and RF links, respectively. The IM/DD was considered for the FSO link. In [16], the ergodic capacity of multi-hop hybrid FSO/RF for terrestrial networks was derived, considering Gamma-Gamma and Nakagami-m models for FSO and RF links, respectively. They also assumed a decode-and-forward relaying scheme and IM/DD for the FSO link. The derived capacity expressions were obtained in terms of bivariate Fox's H function for both FSO and RF links. From the previous work, we can conclude that there is no unified capacity analysis that accounts for both types of detection techniques (IM/DD and HD) for FSO link. Further, because of the strong line-of-sight RF component and weak scattered components between a ground station and satellite, Rician distribution can model the RF link more accurately [12], [17].

In this work, we provide a thorough ergodic capacity analysis for the integrated Satcom system in Fig. 1. We derive exact and asymptotic expressions of the ergodic capacity for both IM/DD and HD schemes under Gamma-Gamma and Rician distributions. The main contributions of our work are as follows:

- We derive a new unified exact analytical expression for the ergodic capacity of the FSO link with IM/DD and HD receivers under Gamma-Gamma distribution when the instantaneous received signal-to-noise ratio (SNR) is greater than a predefined threshold. Considering Rician distribution, a new exact expression for the ergodic capacity of the RF link is derived.
- We capitalize on these unified expressions to obtain the ergodic capacity of the Satcom system with integrated SAG-FSO/SH-FSO/RF transmissions. The optimum switching threshold has been determined to maximize the ergodic capacity of the integrated Satcom system.
- Additionally, we derive asymptotic expressions for the ergodic capacity that are computationally less intensive to gain useful insights for engineering applications.
- Through a selected numerical example, we show that

the integrated Satcom system with IM/DD can achieve a capacity gain over that with HD technique over all satellite zenith angles, which is against popular belief.

The rest of this paper is organized as follows. The system and channel models are presented in Section II. The ergodic capacity of the integrated Satcom system is analyzed in Section III, which leads to both exact and asymptotic results. The numerical results are presented in Section IV. Finally, Section V concludes our work.

II. System and Channel Models

The integrated Satcom system combines the SAG-FSO transmission with conventional hybrid SH-FSO/RF transmission to create a high-throughput and reliable Satcom system. As shown in Fig. 1, the system includes a ground station with two optical transmitters and an RF transmitter, a HAP, dispatched directly above the ground station at a small zenith angle and acting as an FSO relay, and a satellite with FSO and RF receivers. Two optical transmitters at the ground station are used to minimize the switching time between SAG-FSO and SH-FSO transmissions. Specifically, one optical transmitter (OTx_1) will target the HAP relay, and the other (OTx_2) is dedicated to the direct FSO transmission to the satellite. Note that FSO links may experience similar small-scale fading if the spacing between the two optical transmitters is smaller than the atmospheric coherence diameter. Therefore, the spacing between transmitters for ground-to-SAT (GS) and ground-to-HAP (GH) links is maintained at a sufficiently large distance for uncorrelated small-scale fading [18]. For the given system configuration, we need a spacing of about 20 cm between the optical transmitters [18, eq. (8)]. The required spacing is perfectly feasible, considering the size of the ground station's operating sites. For large-scale fading, as long as the satellite zenith angle is not too small, the two FSO links will have a higher probability of experiencing independent large-scale fading. Given that GEO satellites are deployed at 38,000 km above the earth's equator and that one GEO satellite may cover one-third of the earth's surface, the satellite zenith angle is large for most ground stations, except those located at or near the equator[1]. For LEO, the satellite zenith angle will be small if the satellite pass is at nadir or near to nadir for a given ground station, which is a small portion of the whole communication session. Therefore, we assume independent fading for SAG-FSO and SH-FSO transmissions in the following analysis, and the effect of correlation will be investigated in future work.

In this work, we adopt a single-threshold hard-switching scheme to switch between different links. We prioritize the SAG-FSO link due to its better performance compared to the SH-FSO link, i.e., SAG-FSO performance is insensitive to satellite zenith angle variation [13]. The integrated Satcom system will use the SAG-FSO link as long as its link quality is acceptable, i.e. the instantaneous received SNRs of both hops are above a predefined threshold γ_{th}. When the SAG-FSO link becomes unacceptable, indicated by 1-bit feedback, the system will check the received SNR of the SH-FSO link before resorting to the RF link. If the SNRs of all links are below the respective threshold, an outage will be declared. We assume sub-carrier intensity modulation (SIM) with M-ary phase-shift-keying (MPSK) for FSO transmissions and IM/DD or HD at the receiver to detect the received optical signal. Furthermore, the MPSK modulation is adopted for the RF link.

[1]In equatorial regions, using HAP with FSO relaying capabilities may not be worthwhile since the SAG-FSO link will experience a similar amount of atmospheric turbulence as SH-FSO transmission.

A. FSO channel model

We assume that FSO transmissions experience Gamma-Gamma fading with pointing error and weather impairments. The probability density function (pdf) of the receiver irradiances I_{xy}, $\mathrm{xy} \in \{\mathrm{GH}, \mathrm{HS}, \mathrm{GS}\}$, are given by [19, eq. (1)]

$$f_{I_{\mathrm{xy}}}(I) = \frac{\xi_{\mathrm{xy}}^2 \; I^{-1}}{\Gamma(\alpha_{\mathrm{xy}})\Gamma(\beta_{\mathrm{xy}})} G_{1,3}^{3,0}\left(\alpha_{\mathrm{xy}}\beta_{\mathrm{xy}} \frac{I}{A_0 \; I_{\mathrm{xy}}^l} \;\middle|\; \begin{matrix} \xi_{\mathrm{xy}}^2 + 1 \\ \xi_{\mathrm{xy}}^2, \alpha_{\mathrm{xy}}, \beta_{\mathrm{xy}} \end{matrix}\right), \tag{1}$$

where ξ_{xy} is the ratio between the equivalent beam radius and the pointing error displacement standard deviation (jitter) at the receiver, A_0 is the fraction of total power collected at the receiver aperture, I_{xy}^l is the atmospheric attenuation due to different weather conditions and is defined by Beer-Lambert law [6], $\Gamma(.)$ is the Gamma function as defined in [20, eq. (8.310)], $\mathrm{G}(.)$ is the Meijer's G function as defined in [20, eq. (9.301)], and α_{xy} and β_{xy} are the large-scale and small-scale fading parameters of atmospheric turbulence. Note that α_{xy} and β_{xy} for Satcom uplink follows [21, eq. (7a, 7b)], and for the downlink [22, eq. (7-10)]. The main difference is the beam-wander-induced pointing error effect. Beam wander occurs when the size of the beam is smaller than the size of the eddies. For the uplink, the beam encounters turbulence near the transmitter. Thus, its diameter will be smaller than the eddy size. So, the beam gets deflected from its original path, leading to pointing error and performance deterioration. For the downlink, the effect of the beam wander is negligible, as the beam diameter is much larger than the turbulent eddy size when the beam reaches the atmosphere [6].

The instantaneous and average SNRs at the FSO receiver with HD or IM/DD are given by [11, eq. (7, 10)]

$$\gamma_{\mathrm{xy},b} = \frac{(\eta_{\mathrm{xy}} \; P_{\mathrm{xy}} \; G_{\mathrm{x}}^{\mathrm{tx}} \; G_{\mathrm{y}}^{\mathrm{rx}} \; I_{\mathrm{xy}})^b}{\mathrm{FL}_{\mathrm{xy}}^b \; \sigma_{n_{\mathrm{xy}}}^2}, \tag{2}$$

and,

$$\bar{\gamma}_{\mathrm{xy},b} = \frac{(\eta_{\mathrm{xy}} \; P_{\mathrm{xy}} \; G_{\mathrm{x}}^{\mathrm{tx}} \; G_{\mathrm{y}}^{\mathrm{rx}} \; k_{\mathrm{xy}} \; I_{xy}^l \; A_0)^b}{\mathrm{FL}_{\mathrm{xy}}^b \; \sigma_{n_{\mathrm{xy}}}^2}, \tag{3}$$

respectively, where $k_{\mathrm{xy}} = \xi_{\mathrm{xy}}^2/(\xi_{\mathrm{xy}}^2 + 1)$, η_{xy} represents the optical-to-electrical efficiency of the optical receiver, P_{xy} denotes the optical average transmit power, $G_{\mathrm{x}}^{\mathrm{tx}}$ denotes the transmit telescope gain, $G_{\mathrm{y}}^{\mathrm{rx}}$ represents the telescope gain at the receiver, $\mathrm{FL}_{\mathrm{xy}}$ is the free-space loss of the FSO link, $\sigma_{n_{\mathrm{xy}}}^2$ is the variance of additive white Gaussian noise (AWGN) over the FSO link, and b is the parameter which depends on the type of detection used (i.e. $b = 1$ for HD and $b = 2$ for IM/DD). Therefore, a unified expression of the pdf of the instantaneous

SNR including both HD and IM/DD can be derived from (1) as [23, eq. (2)]

$$f_{\gamma_{\rm xy}}(\gamma) = \frac{\xi_{\rm xy}^2\ \gamma^{-1}}{b\ \Gamma(\alpha_{\rm xy})\Gamma(\beta_{\rm xy})} \times G_{1,3}^{3,0}\left(\frac{\alpha_{\rm xy}\beta_{\rm xy}k_{\rm xy}}{I_{\rm xy}^l}\left(\frac{\gamma}{\mu_{{\rm xy},b}}\right)^{\frac{1}{b}}\middle|\ \begin{matrix}\xi_{\rm xy}^2+1\\ \xi_{\rm xy}^2,\alpha_{\rm xy},\beta_{\rm xy}\end{matrix}\right), \quad (4)$$

where $\mu_{{\rm xy},b}$ denotes the average electrical SNR, related to the average SNR at the FSO receiver $\bar{\gamma}_{{\rm xy},b}$ as

$$\mu_{\rm xy,1} = \bar{\gamma}_{\rm xy,1},$$

and

$$\mu_{\rm xy,2} = \frac{\alpha_{\rm xy}\,\beta_{\rm xy}\,\xi_{\rm xy}^2\,(\xi_{\rm xy}^2+2)}{(\alpha_{\rm xy}+1)(\beta_{\rm xy}+1)(\xi_{\rm xy}^2+1)^2}\ \bar{\gamma}_{\rm xy,2}.$$

B. RF Channel model

Because of a strong line-of-sight and weak scattered components between transmitter and receiver in Satcom, the RF signal experiences minimal scattering and reflection from the environment. Therefore, the small-scale fading channel coefficient ($h_{\rm RF}$) of the RF link can be characterized using the Rician distribution, where the non-zero mean represents the presence of a strong line-of-sight component. The pdf of the instantaneous SNR is given by [24, eq. (2.16)]

$$f_{\gamma_{\rm RF}}(\gamma) = \frac{K+1}{\bar{\gamma}_{\rm RF}}\ \exp\left(-(K+1)\ \frac{\gamma}{\bar{\gamma}_{\rm RF}} - K\right) \times I_0\left(2\ \sqrt{K(K+1)\ \frac{\gamma}{\bar{\gamma}_{\rm RF}}}\right), \quad (5)$$

where $I_0(.)$ is the zeroth-order modified Bessel function of the first kind and K denotes the Rician parameter, which is the ratio of the power in the line-of-sight path to the power in scattered paths. The average SNR $\bar{\gamma}_{\rm RF}$ is represented by [25, eq. (5.34)]

$$\bar{\gamma}_{\rm RF} = \frac{P_{\rm RF}\ G_{\rm RF}^{\rm tx}\ G_{\rm RF}^{\rm rx}}{{\rm FL}_{\rm RF}\ {\rm L_o}\ \sigma_{n_{\rm RF}}^2}, \quad (6)$$

where $P_{\rm RF}$ denotes the average transmit power of the RF link, $G_{\rm RF}^{\rm tx}$ and $G_{\rm RF}^{\rm rx}$ indicate the antenna gains (transmit and receive), ${\rm FL}_{\rm RF}$ is the free-space loss, $\sigma_{n_{\rm RF}}^2$ represents variance of the thermal noise at the RF receiver and is modelled by AWGN, and ${\rm L_o}$ represents other losses due to rain, atmospheric gaseous such as oxygen, polarization, and mispointing.

Applying series expansion to the modified Bessel function using [20, eq. (8.447.1)], the pdf in (5) can be rewritten as

$$f_{\gamma_{\rm RF}}(\gamma) = \mathcal{F}\exp(-K)\exp(-\mathcal{F}\gamma)\sum_{m=0}^{\infty}\frac{(K\mathcal{F})^m}{(m!)^2}\ \gamma^m, \quad (7)$$

where $\mathcal{F} = \frac{K+1}{\bar{\gamma}_{\rm RF}}$.

III. Ergodic Capacity Analysis

We now analyze the ergodic capacity of the integrated Satcom system with consideration of the pointing error effect and derive both exact and simpler asymptotic expressions.

A. Exact analysis

The ergodic capacity of the Satcom system in Fig. 1 can be calculated as

$$\bar{C}^{\rm Satcom} = \bar{C}^{\rm SAG} + P_{\rm out}^{\rm SAG}\ \bar{C}^{\rm GS\text{-}h}, \quad (8)$$

where $P_{\rm out}^{\rm SAG}$ indicates the outage probability of the SAG-FSO link, $\bar{C}^{\rm SAG}$ and $\bar{C}^{\rm GS\text{-}h}$ are the ergodic capacities of SAG-FSO and hybrid SH-FSO/RF links, respectively.

The SAG-FSO link will be in outage if the instantaneous SNR of either ground-to-HAP or HAP-to-SAT hops is below the threshold $\gamma_{\rm th}$. Therefore, $P_{\rm out}^{\rm SAG}$ is given by

$$P_{\rm out}^{\rm SAG} = 1 - \left(1 - P_{\rm out}^{\rm GH}\right)\left(1 - P_{\rm out}^{\rm HS}\right), \quad (9)$$

where $P_{\rm out}^{\rm GH}$ and $P_{\rm out}^{\rm HS}$ are the outage probabilities of ground-to-HAP and HAP-to-SAT hops, respectively. $P_{\rm out}^{\rm GH}$ can be expressed with the application of (4) and [26, eq. (07.34.21.0084.01)], and some algebraic manipulations, as

$$P_{\rm out}^{\rm GH} = \mathcal{A}_{\rm GH}\ G_{b+1,\ 3b+1}^{\ 3b,\ 1}\left(\mathcal{D}_{\rm GH}\ \frac{\gamma_{\rm th}}{\mu_{{\rm GH},b}}\middle|\ \begin{matrix}1\ ,\ \mathcal{B}_{\rm GH}^1\\ \mathcal{B}_{\rm GH}^2\ ,\ 0\end{matrix}\right), \quad (10)$$

where $\mathcal{A}_{\rm GH} = \frac{b^{\alpha_{\rm GH}+\beta_{\rm GH}-2}\ \xi_{\rm GH}^2}{(2\pi)^{b-1}\ \Gamma(\alpha_{\rm GH})\Gamma(\beta_{\rm GH})}$, $\mathcal{D}_{\rm GH} = \left(\frac{\alpha_{\rm GH}\beta_{\rm GH}k_{\rm GH}}{b^2\ I_{\rm GH}^l}\right)^b$, $\mathcal{B}_{\rm GH}^1 = \{\frac{\xi_{\rm GH}^2+1}{b},\ldots,\frac{\xi_{\rm GH}^2+b}{b}\}$ comprises of b terms, and $\mathcal{B}_{\rm GH}^2 = \{\frac{\xi_{\rm GH}^2}{b},\ldots,\frac{\xi_{\rm GH}^2+b-1}{b},\frac{\alpha_{\rm GH}}{b},\ldots,\frac{\alpha_{\rm GH}+b-1}{b},\frac{\beta_{\rm GH}}{b},\ldots,\frac{\beta_{\rm GH}+b-1}{b}\}$ comprises of $3b$ terms. Similarly, $P_{\rm out}^{\rm HS}$ can be obtained with the corresponding parameters $\alpha_{\rm HS}$, $\beta_{\rm HS}$, $\xi_{\rm HS}$, and $\mu_{{\rm HS},b}$. Since HAP will be usually deployed at a cloud-free atmospheric altitude, the atmospheric attenuation for the HAP-to-SAT hop due to varying weather conditions will be almost equal to unity.

In this work, we adopt a decode-and-forward FSO relaying scheme to eliminate the noise at the relay [27]. Therefore, the end-to-end capacity of the SAG-FSO transmission scheme is given by [16, eq. (16)]

$$\bar{C}^{\rm SAG} = \min\left\{\bar{C}^{\rm GH}\ ,\ \bar{C}^{\rm HS}\right\}, \quad (11)$$

where $\bar{C}^{\rm GH}$ and $\bar{C}^{\rm HS}$ denote the capacity of the ground-to-HAP and HAP-to-SAT FSO links when their instantaneous SNR is greater than $\gamma_{\rm th}$. The threshold is selected to satisfy a certain quality-of-service requirement, typically in terms of target bit error rate (BER). $\bar{C}^{\rm GH}$ can be calculated as

$$\begin{aligned}\bar{C}^{\rm GH} &= \int_{\gamma_{\rm th}}^{\infty} BW_{\rm FSO}\log_2(1+\epsilon\ \gamma)\ f_{\gamma_{\rm GH}}(\gamma)\ d\gamma\\ &= \underbrace{\frac{BW_{\rm FSO}}{\ln(2)}\int_0^{\infty}\ln(1+\epsilon\ \gamma)\ f_{\gamma_{\rm GH}}(\gamma)\ d\gamma}_{I_1}\\ &\quad\underbrace{-\frac{BW_{\rm FSO}}{\ln(2)}\int_0^{\gamma_{\rm th}}\ln(1+\epsilon\ \gamma)\ f_{\gamma_{\rm GH}}(\gamma)\ d\gamma}_{I_2}, \end{aligned} \quad (12)$$

where $BW_{\rm FSO}$ is the bandwidth of the FSO link and ϵ is a constant such that $\epsilon = 1$ for HD technique and $\epsilon = e/(2\pi)$ for

IM/DD technique. Note that the expression in (12) is an exact solution for HD, while it is a lower bound for IM/DD [19].

To evaluate the integral I_1, we rewrite $\ln(1+\epsilon\gamma)$ into a Meijer G-function using [26, eq. (07.34.03.0456.01)]. The analytical expression of I_1 is obtained after some algebraic manipulations, using (4) and [26, eq. (07.34.21.0013.01)] as

$$I_1 = \frac{BW_{\text{FSO}}\ \mathcal{A}_{\text{GH}}}{\ln(2)}\ G_{b+2,\ 3b+2}^{\ 3b+2,\ 1}\left(\frac{\mathcal{D}_{\text{GH}}}{\epsilon\ \mu_{\text{GH},b}}\ \middle|\ \begin{matrix} 0,\ 1\ ,\ \mathcal{B}_{\text{GH}}^{1} \\ \mathcal{B}_{\text{GH}}^{2}\ ,\ 0,\ 0 \end{matrix}\right). \quad (13)$$

To evaluate the integral I_2, $\ln(1+\epsilon\ \gamma)$ is replaced by its Taylor series as (see Appendix A)

$$\ln(1+\epsilon\ \gamma) = \ln(1+\epsilon\ a)\ +\ \sum_{u=1}^{\infty}\frac{(-1)^{u+1}\ \epsilon^u}{u\ (1+\epsilon\ a)^u} \sum_{v=0}^{u}\binom{u}{v}(-a)^{u-v}\ \gamma^v. \quad (14)$$

Now, I_2 can be expressed in the form of $I_2 = I_{2_A} + I_{2_B}$, as

$$I_{2A} = \frac{BW_{\text{FSO}}}{\ln(2)}\int_0^{\gamma_{\text{th}}}\ln(1+\epsilon\ a)\ f_{\gamma_{\text{GH}}}(\gamma)\ d\gamma, \quad (15)$$

and,

$$I_{2B} = \frac{BW_{\text{FSO}}}{\ln(2)}\int_0^{\gamma_{\text{th}}}\ \sum_{u=1}^{\infty}\frac{(-1)^{u+1}\ \epsilon^u}{u\ (1+\epsilon\ a)^u} \sum_{v=0}^{u}\binom{u}{v}\ (-a)^{u-v}\ \gamma^v\ f_{\gamma_{\text{GH}}}(\gamma)\ d\gamma, \quad (16)$$

respectively. By using (4), (15), (16), and [26, eq. (07.34.21.0084.01)], the analytical expressions of I_{2_A} and I_{2_B} are given by

$$I_{2_A} = BW_{\text{FSO}}\ \log_2(1+\epsilon\ a)\ P_{\text{out}}^{\text{GH}}, \quad (17)$$

and,

$$I_{2_B} = \frac{BW_{\text{FSO}}\mathcal{A}_{\text{GH}}}{\ln 2}\sum_{u=1}^{\infty}\frac{(-1)^{u+1}\ \epsilon^u}{u(1+\epsilon\ a)^u}\sum_{v=0}^{u}\binom{u}{v}(-a)^{u-v}\ \gamma_{\text{th}}^{v} \times G_{b+1,\ 3b+1}^{\ 3b,\ 1}\left(\mathcal{D}_{\text{GH}}\ \frac{\gamma_{\text{th}}}{\mu_{\text{GH},b}}\ \middle|\ \begin{matrix} 1-v\ \ ,\ \mathcal{B}_{\text{GH}}^{1} \\ \mathcal{B}_{\text{GH}}^{2}\ \ ,\ -v \end{matrix}\right), \quad (18)$$

respectively. Note that convergence of the infinite summation in (18) is guaranteed if the SNR satisfies the ratio test in (34). Since γ_{th} is typically small, we can select an a value to satisfy the convergence condition. The expression of $\bar{C}^{\text{HS}}$ can be obtained similar to (12), using the corresponding parameters α_{HS}, β_{HS}, ξ_{HS}, and $\mu_{\text{HS},b}$. Then, $\bar{C}^{\text{SAG}}$ in (11) can be analytically evaluated.

The ergodic capacity of the hybrid SH-FSO/RF transmission scheme can be computed as [8, eq. (3)]

$$\bar{C}^{\text{GS-h}} = \bar{C}^{\text{GS}}\ +\ P_{\text{out}}^{\text{GS}}\ \ \bar{C}^{\text{RF}}, \quad (19)$$

where $P_{\text{out}}^{\text{GS}}$ indicates the outage probability of the SH-FSO that can be represented as (10) using the corresponding parameters α_{GS}, β_{GS}, ξ_{GS}, and $\mu_{\text{GS},b}$ values. $\bar{C}^{\text{GS}}$ indicates the capacity of the SH-FSO when $\gamma_{\text{GS}} \geq \gamma_{\text{th}}$ and can be defined as in (12).

Eventually, the capacity of the RF link when $\gamma_{\text{RF}} \geq \gamma_{\text{th}}$ can be expressed as

$$\bar{C}^{\text{RF}} = \underbrace{\frac{BW_{\text{RF}}}{\ln(2)}\int_0^{\infty}\ln(1+\gamma)\ f_{\gamma_{\text{RF}}}(\gamma)\ d\gamma}_{I_3} - \underbrace{\frac{BW_{\text{RF}}}{\ln(2)}\int_0^{\gamma_{\text{th}}}\ln(1+\gamma)\ f_{\gamma_{\text{RF}}}(\gamma)\ d\gamma}_{I_4}, \quad (20)$$

where BW_{RF} is the bandwidth of the RF link. To evaluate integrals I_3 and I_4 , we first rewrite $\ln(1+\gamma)$ in (20) into a Meijer G-function using [26, eq. (07.34.03.0456.01)]. Then, the analytical expression of I_3 is obtained after some algebraic manipulations, using (7), [26, eq. (07.34.21.0088.01)], and [20, eq. (9.31.2)] as

$$I_3 = \frac{BW_{\text{RF}}}{\ln(2)}\ \exp(-K)\ \sum_{m=0}^{\infty}\frac{K^m}{(m!)^2} \times G_{2,3}^{3,1}\left(\frac{K+1}{\bar{\gamma}_{\text{RF}}}\ \middle|\ \begin{matrix} 0\ \ ,\ \ 1 \\ 1+m, 0, 0 \end{matrix}\right). \quad (21)$$

For the integral I_4, we replace $\exp(-\mathcal{F}\gamma)$ in (7) by its series expansion using [20, eq. (1.211.1)]. By using [26, eq. (07.34.21.0084.01)] and [20, eq. (9.31.2)], the expression of I_4 is given by

$$I_4 = \frac{BW_{\text{RF}}\ \mathcal{F}}{\ln(2)}\ \exp(-K)\sum_{n=0}^{\infty}\frac{(-\mathcal{F})^n}{n!}\ \sum_{m=0}^{\infty}\frac{(K\mathcal{F})^m}{(m!)^2}\ \gamma_{\text{th}}^{\tau} \times\ G_{3,3}^{3,1}\left(\frac{1}{\gamma_{\text{th}}}\ \middle|\ \begin{matrix} 0, 1, 1+\tau \\ \tau\ ,\ 0\ ,\ 0 \end{matrix}\right), \quad (22)$$

where $\tau = m+n+1$. It is worth noting that the terms in the infinite summations of (21) and (22) decrease at the rate of $\frac{1}{(m!)^2}$ or $\frac{1}{n!}$, ensuring their convergence.

B. Asymptotic Analysis

In this section, we drive a simpler asymptotic expression for the ergodic capacity of the integrated Satcom system at higher SNRs by applying the asymptotic expansion of the Meijer G-function in terms of basic elementary functions, given in Appendix B. The asymptotic ergodic capacity can be expressed by

$$\bar{C}_a^{\text{Satcom}} = \min\left\{\bar{C}_a^{\text{GH}}, \bar{C}_a^{\text{HS}}\right\}\ +\ \left[1-\left(1-P_{a\text{out}}^{\text{GH}}\right)\left(1-P_{a\text{out}}^{\text{HS}}\right)\right] \times\left[\bar{C}_a^{\text{GS}}\ +\ P_{a\text{out}}^{\text{GS}}\ \ \bar{C}_a^{\text{RF}}\right]. \quad (23)$$

The asymptotic outage expression of the ground-to-HAP link is obtained with the application of [20, eq. (9.303)] and (10) as

$$P_{a\text{out}}^{\text{GH}} = \sum_{g=1}^{3b}\ \frac{\mathcal{A}_{\text{GH}}}{\mathcal{B}_{\text{GH}}^{2,g}}\ \mathcal{X}_1\ \left(\frac{\mathcal{D}_{\text{GH}}\ \gamma_{\text{th}}}{\mu_{\text{GH},b}}\right)^{\mathcal{B}_{\text{GH}}^{2,g}}, \quad (24)$$

where $\mathcal{X}_1 = \frac{\prod_{j=1;j\neq g}^{3b}\Gamma\left(\mathcal{B}_{\text{GH}}^{2,j}-\mathcal{B}_{\text{GH}}^{2,g}\right)}{\prod_{j=1}^{b}\Gamma\left(\mathcal{B}_{\text{GH}}^{1,j}-\mathcal{B}_{\text{GH}}^{2,g}\right)}$. Similarly, $P_{a\text{out}}^{\text{HS}}$ and $P_{a\text{out}}^{\text{GS}}$ can be obtained, using the corresponding parameters α_{xy}, β_{xy}, ξ_{xy}, and $\mu_{\text{xy},b}$.

The asymptotic ergodic capacity of the ground-to-HAP link can be written as $\bar{C}_a^{\text{GH}} = I_1^a - I_{2_A}^a - I_{2_B}^a$, where

$$I_1^a = \frac{BW_{\text{FSO}}\ \mathcal{A}_{\text{GH}}}{\ln(2)} \sum_{g=1}^{3b+2} \mathcal{X}_2\ \frac{\Gamma\left(1+\mathcal{B}_{\text{GH}}^{3,g}\right)}{\Gamma\left(1-\mathcal{B}_{\text{GH}}^{3,g}\right)} \left(\frac{\mathcal{D}_{\text{GH}}}{\epsilon\ \mu_{\text{GH},b}}\right)^{\mathcal{B}_{\text{GH}}^{3,g}}, \quad (25)$$

$$I_{2_A}^a = BW_{\text{FSO}}\ \log_2(1+\epsilon\ a)\ P_{a\text{out}}^{\text{GH}}, \quad (26)$$

and

$$I_{2_B}^a = \frac{BW_{\text{FSO}}\ \mathcal{A}_{\text{GH}}}{\ln(2)} \sum_{g=1}^{3b} \mathcal{X}_1\ \left(\frac{\mathcal{D}_{\text{GH}}\ \gamma_{\text{th}}}{\mu_{\text{GH},b}}\right)^{\mathcal{B}_{\text{GH}}^{2,g}} \sum_{u=1}^{\infty} \frac{(-1)^{u+1}\ \epsilon^u}{u(1+\epsilon\ a)^u} \sum_{v=0}^{u} \binom{u}{v}\ (-a)^{u-v}\ \frac{\gamma_{\text{th}}^v}{v+\mathcal{B}_{\text{GH}}^{2,g}}. \quad (27)$$

Here, we define $\mathcal{X}_2 = \frac{\prod_{j=1;j\neq g}^{3b+2}\Gamma\left(\mathcal{B}_{\text{GH}}^{3,j}-\mathcal{B}_{\text{GH}}^{3,g}\right)}{\prod_{j=1}^{b}\Gamma\left(\mathcal{B}_{\text{GH}}^{1,j}-\mathcal{B}_{\text{GH}}^{3,g}\right)}$ and $\mathcal{B}_{\text{GH}}^{3,g} = \{\mathcal{B}_{\text{GH}}^{2,g}, 0, 0\}$. Similarly, $\bar{C}_a^{\text{HS}}$ and $\bar{C}_a^{\text{GS}}$ can be obtained, using the corresponding parameters α_{xy}, β_{xy}, ξ_{xy}, and $\mu_{\text{xy},b}$.

The asymptotic ergodic capacity of the RF link can be written as $\bar{C}_a^{\text{RF}} = I_3^a - I_4^a$, where

$$I_3^a = \frac{BW_{\text{RF}}}{\ln(2)}\ \exp(-K) \sum_{m=0}^{\infty} \frac{(K)^m}{(m!)^2} \sum_{g=1}^{3} \mathcal{X}_3\ \frac{\Gamma\left(1+\mathcal{B}_{\text{RF}}^{4,g}\right)}{\Gamma\left(1-\mathcal{B}_{\text{RF}}^{4,g}\right)} \left(\frac{K+1}{\bar{\gamma}_{\text{RF}}}\right)^{\mathcal{B}_{\text{RF}}^{4,g}}, \quad (28)$$

and

$$I_4^a = \frac{BW_{\text{RF}}\ \mathcal{F}}{\ln(2)}\ \exp(-K) \sum_{n=0}^{\infty} \frac{(-\mathcal{F})^n}{n!} \sum_{m=0}^{\infty} \frac{(K\mathcal{F})^m}{(m!)^2}\ \gamma_{\text{th}}^{\tau} \sum_{g=1}^{3} \mathcal{X}_4\ \frac{\Gamma\left(1+\mathcal{B}_{\text{RF}}^{5,g}\right)}{\Gamma\left(1-\mathcal{B}_{\text{RF}}^{5,g}\right)} \left(\frac{1}{\gamma_{\text{th}}}\right)^{\mathcal{B}_{\text{RF}}^{5,g}}. \quad (29)$$

Here, we define $\mathcal{X}_3 = \prod_{j=1;j\neq g}^{3}\Gamma\left(\mathcal{B}_{\text{RF}}^{4,j}-\mathcal{B}_{\text{RF}}^{4,g}\right)$, $\mathcal{B}_{\text{RF}}^{4,g} = \{1+m, 0, 0\}$, $\mathcal{X}_4 = \frac{\prod_{j=1;j\neq g}^{3}\Gamma\left(\mathcal{B}_{\text{RF}}^{5,j}-\mathcal{B}_{\text{RF}}^{5,g}\right)}{\Gamma\left(1+\tau-\mathcal{B}_{\text{RF}}^{5,g}\right)}$, and $\mathcal{B}_{\text{RF}}^{5,g} = \{\tau, 0, 0\}$.

Note that the derived ergodic capacity expressions are valid for both uplink and downlink Satcom scenarios by using the appropriate expressions for α_{xy}.

IV. Numerical Results

We present selected numerical results to illustrate the ergodic capacity performance of the integrated Satcom system. System parameters will be the same as listed in Table I unless otherwise indicated. For presentation clarity and comparison purposes, we assume that ground-to-HAP, ground-to-SAT, and HAP-to-SAT FSO links have the same average received SNR without losing generality. As such, each FSO link may have a different transmit power. Also, we assume an uplink scenario, an IM/DD scheme (except for Fig. 5), and the same average SNR of the RF link as the average SNR of the FSO link (i.e., $\bar{\gamma}_{\text{RF}} = \bar{\gamma}_{\text{GS}}$). It should be noted that the zenith angles (θ_{HS} and θ_{GS}) vary with the satellite's position, whereas for θ_{GH}, it is maintained at a low/fixed value of 5°. The truncation limits for infinite summations are considered $u = 30$, $n = 20$, and $m = 20$ as greater values have a negligible effect on the ergodic capacity values.

TABLE I
Simulation Parameters

Parameter	*Symbol*	*Value*
FSO wavelength	λ	1550 nm
FSO link bandwidth	BW_{FSO}	1 GHz
Satellite altitude	h_{S}	620 km
HAP altitude	h_{H}	20 km
GS aperture height	h_{G}	1 m
Pointing error coefficients	ξ_{GS}, ξ_{GH}, and ξ_{HS}	5.2, 5.2, and 13.07
Wind speed	ω	21 m/s
Ground level turbulence	$C_{\text{n}}^2(0)$	$1.7\times10^{-14}\text{m}^{\frac{-2}{3}}$
Satellite zenith angle: HAP-to-SAT, ground-to-SAT	θ_{HS}, θ_{GS}	30° : 80°
HAP zenith angle: ground-to-HAP	θ_{GH}	5°
Beam radius at transmitter	W_0^{G}, W_0^{H}	0.02 m
Optical-to-electrical efficiency	η	0.8
Switching threshold	γ_{th}	10.5 dB
Rician factor	K	6
RF link bandwidth	BW_{RF}	300 MHz

Fig. 2(a) shows the ergodic capacity performance of the integrated Satcom system together with several other Satcom transmission schemes for a fixed satellite zenith angle of 80°. We can observe that the asymptotic results closely match the exact expressions at high-SNR values. Also, the analytical results match the Monte-Carlo simulations perfectly. Further, the integrated Satcom system achieves the best performance over all SNR values. It can achieve capacity gains of about 2 Gbps and 2.3 Gbps over hybrid SAG-FSO/RF in [11] and hybrid SH-FSO/RF in [8], respectively, at an average SNR of 30 dB. This performance advantage originates from the minimization of the atmospheric turbulence effect with the low-zenith-angle considered for the ground-to-HAP transmission. The frequency of switching to the RF link is also reduced to a large extent, which increases the overall system throughput.

In Fig. 2(b) we plot the ergodic capacity as a function of satellite zenith angles with an average link SNR of 15 dB. The capacity performance of the SH-FSO transmission scheme degrades dramatically, from 3.8 Gbps to 1.7 Gbps as the zenith angle increases from 30° to 80°. The capacity of both hybrid SAG-FSO/RF [11] and hybrid SH-FSO/RF [8] exhibits a similar degradation trend as the zenith angle increases, but with a certain performance improvement. The capacity performance of the integrated Satcom system only slightly deteriorates with the increase in satellite zenith angle. This result supports the fact that the long propagation distance through the atmosphere has an impact on the SH-FSO link. Despite the slight capacity variation, the integrated Satcom system outperforms other transmission schemes over all satellite zenith angles.

This article has been accepted for publication in IEEE Photonics Journal. This is the author's version which has not been fully edited and content may change prior to final publication. Citation information: DOI 10.1109/JPHOT.2022.3201046

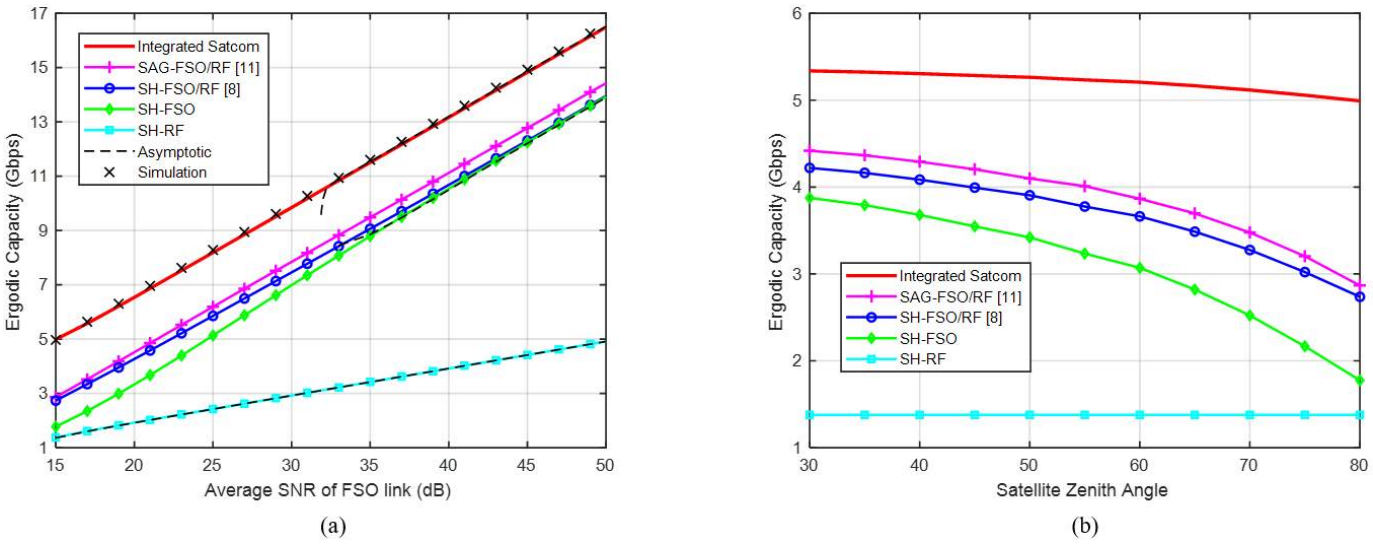

Fig. 2. Ergodic capacity comparison of Satcom transmission systems.

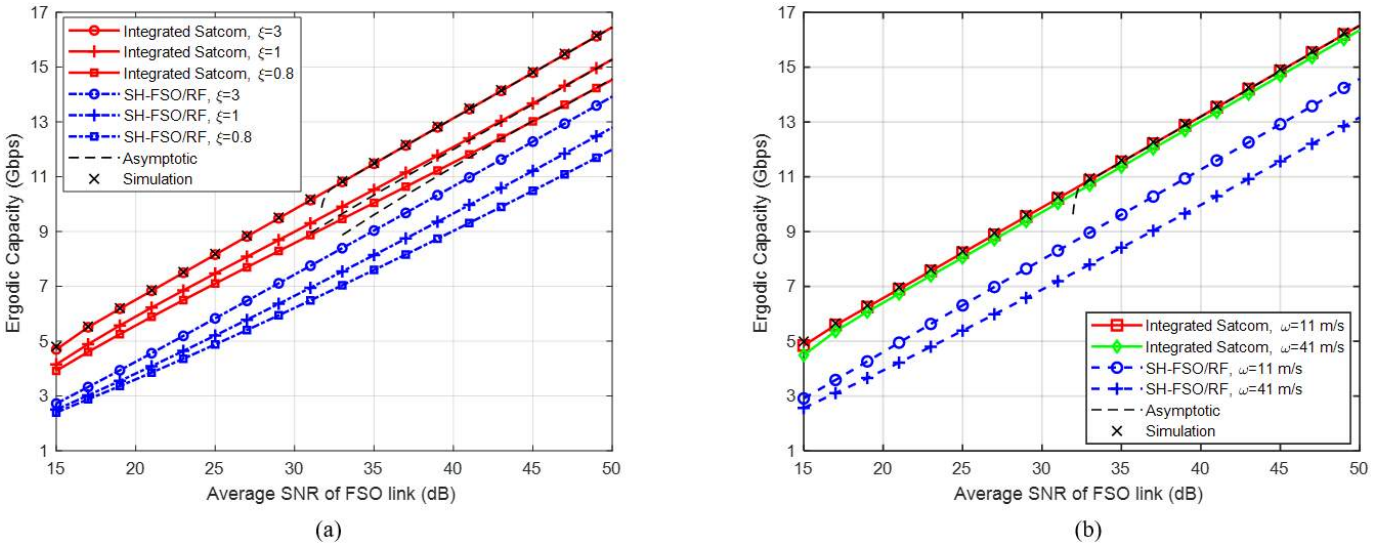

Fig. 3. Ergodic capacity performance of the integrated Satcom : (a) Effect of pointing errors, (b) Effect of wind.

In Fig. 3(a), we investigate the effect of pointing errors with various pointing error coefficient values (i.e., ξ = 0.8, ξ = 1, and ξ = 3) and a fixed satellite zenith angle of 80°. As we can see, the ergodic capacity performance is negatively affected by the decrease in ξ value. For example, the integrated Satcom system suffers a performance loss of about 1 Gbps when ξ decreases from 3 to 0.8, at an average SNR of 25 dB. Most importantly, even under such severe pointing error effects (i.e., ξ = 0.8), the integrated Satcom system maintains a performance advantage over the hybrid SH-FSO/RF system for a wide range of SNRs.

The capacity performances of the integrated Satcom and hybrid SH-FSO/RF are compared in Fig. 3(b) for various wind speeds, assuming an 80° satellite zenith angle. Note that higher wind speeds increase the formation of vortexes in the air. This phenomenon will effectively change the refractive index of the air, which will cause beam-wander-induced pointing errors and higher fluctuations in the received signal amplitude. Thus, degradation in capacity performance will occur. From this figure, we can find that the wind speed impacts the performance of the hybrid SH-FSO/RF system to a greater extent compared to the integrated Satcom system. The hybrid SH-FSO/RF system's ergodic capacity decreases by about 1 Gbps when the wind speed increases from 11 m/s to 41 m/s, at an average SNR of 25 dB. On the other hand, the integrated Satcom system encounters negligible degradation from such variations in wind speed, thanks to the integrated Satcom system's reliable architecture.

In Fig. 4, we study the optimum threshold selection for the SAG-FSO link, denoted by $\gamma_{\text{th}}^{\text{SAG}}$, for the best integration with the hybrid SH-FSO/RF system. The switching threshold for hybrid SH-FSO/RF, denoted by γ_{th}, is selected to satisfy a certain quality-of-service requirement. Assuming a binary PSK modulation, the switching threshold γ_{th} = 10.5 dB is

This article has been accepted for publication in IEEE Photonics Journal. This is the author's version which has not been fully edited and
content may change prior to final publication. Citation information: DOI 10.1109/JPHOT.2022.3201046

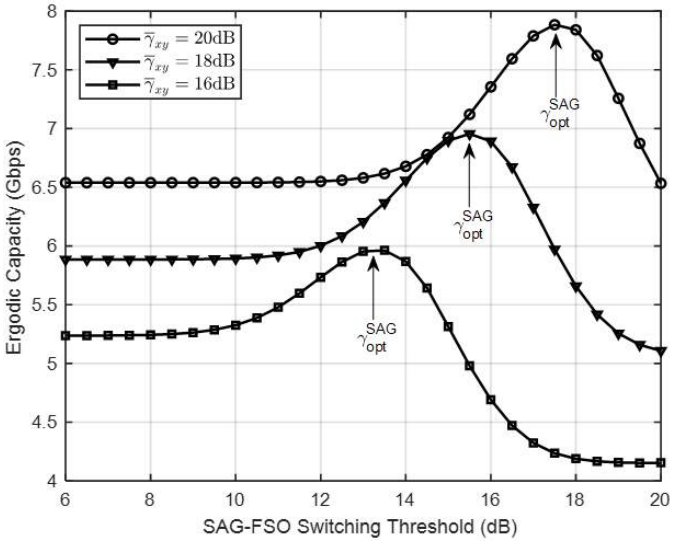

Fig. 4. Optimum switching threshold for the SAG-FSO link.

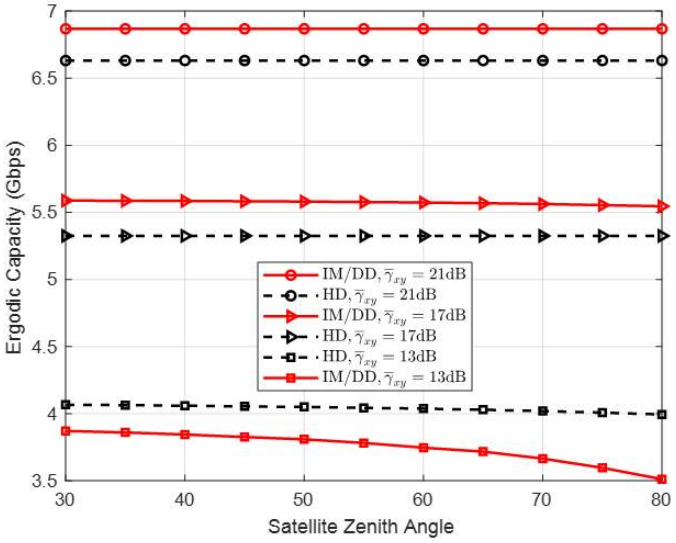

Fig. 5. Ergodic capacity comparison of IM/DD and HD detection techniques with integrated Satcom system.

selected to satisfy a target BER of 10^{-6} [28]. We plot the ergodic capacity of the integrated Satcom system as a function of $\gamma_{\text{th}}^{\text{SAG}}$ for different average SNRs and a fixed satellite zenith angle of 60^{o}. From this figure, we can observe that there is an optimal choice of $\gamma_{\text{th}}^{\text{SAG}}$ in terms of maximizing ergodic capacity, and the optimal value increases with the average SNR. For example, $\gamma_{\text{opt}}^{\text{SAG}}$ equals 13.5 dB and 17.5 dB for average SNRs of 16 dB and 20 dB, respectively.

In Fig. 5, we compare the ergodic capacity of the integrated Satcom system with different detection techniques. From this figure, the integrated Satcom system with IM/DD detection can achieve better performance than with HD over all satellite zenith angles as the received average SNR increases. For example, we can obtain a capacity gain of about 0.3 Gbps over the HD technique at an average SNR of 17 dB. This somewhat surprising result can be explained as follows: HD generally outperforms IM/DD under severe atmospheric turbulence conditions and over low SNRs due to its coherent detection nature. With the proposed SAG-FSO transmission in a low-zenith-angle direction, the adverse effect of atmospheric turbulence will be successfully reduced. Therefore, over a high SNR region, the SAG-FSO with IM/DD can achieve a higher transmission rate than with the HD scheme. For example, the SAG-FSO with IM/DD can maintain a capacity gain of 0.15 Gbps, at an average SNR of 17 dB. Note that the threshold setting has an impact on this behavior. In particular, when the threshold is set too low, the system will use SAG-FSO over a low SNR scenario, where the system with HD outperforms that with IM/DD. The HD technique can also maintain a lower outage probability compared to the IM/DD technique. Therefore, the frequency of switching to the hybrid SH-FSO/RF is lowered compared to the IM/DD case. The SAG-FSO with HD technique has an outage probability of 3.92×10^{-7} that increases to 2.21×10^{-2} in the case of IM/DD, at an average SNR of 17 dB. As such, the Satcom with IM/DD benefits more from the backup SH-FSO/RF links than with the HD detection technique.

V. Conclusion

In this article, we derived exact and asymptotic expressions for the ergodic capacity of the integrated SAG-FSO/SH-FSO/RF Satcom system. We obtained new unified capacity expressions for both FSO and RF links when the instantaneous SNR is greater than a predefined threshold, assuming Gamma-Gamma and Rician fading, respectively. We also investigated the switching threshold optimization to further improve the capacity performance. We showed through selected numerical examples that the integrated transmission system with single-hop and space-air-ground FSO links to the satellite can achieve higher throughput while enjoying high reliability compared to existing solutions. In addition to the ease of implementation and cost-effectiveness, the IM/DD technique can achieve a certain capacity gain over the HD technique for the high-throughput Satcom system under consideration.

Appendix A
Taylor Series Expansion of $\ln(1+\epsilon\,\gamma)$

Here, we derive the Taylor series expansion of $\ln(1+\epsilon\,\gamma)$. First, Taylor's theorem is given by

$$f(x) = \sum_{u=0}^{\infty} f^{(u)}(a)\frac{(x-a)^u}{u!}, \tag{30}$$

where the function of x is expanded about a value, a. Let's expand this summation and replace $f^{(u)}(x)$ by $\ln(1+\epsilon\,\gamma)$ and its derivatives as follow

$$\begin{aligned}\ln(1+\epsilon\gamma) = \ln(1+\epsilon\ a) &+ \frac{\epsilon}{(1+\epsilon a)}\ \frac{(\gamma-a)}{1!} \\ &- \frac{\epsilon^2}{(1+\epsilon a)^2}\ \frac{(\gamma-a)^2}{2!} + \frac{2\ \epsilon^3}{(1+\epsilon a)^3}\ \frac{(\gamma-a)^3}{3!} \\ &- \frac{6\ \epsilon^4}{(1+\epsilon a)^4}\ \frac{(\gamma-a)^4}{4!} + \ldots\end{aligned} \tag{31}$$

After some algebraic manipulations, $\ln(1+\epsilon\ \gamma)$ can be rewritten as

$$\ln(1+\epsilon\ \gamma) = \ln(1+\epsilon\ a)\ +\ \sum_{u=1}^{\infty} \frac{(-1)^{u+1}\ \epsilon^u}{u\ (1+\epsilon\ a)^u} \sum_{v=0}^{u} \binom{u}{v} (-a)^{u-v}\ \gamma^v. \tag{32}$$

Then, the interval of convergence that achieves the ratio test

$$\lim_{u\to\infty} \left| \frac{\mathcal{M}_{u+1}}{\mathcal{M}_u} \right| < 1, \tag{33}$$

where $\mathcal{M}_u = \frac{(-1)^{u+1}\ \epsilon^u}{u(1+\epsilon a)^u}\ (\gamma - a)^u$ and $\mathcal{M}_{u+1} = \frac{(-1)^{u+2}\ \epsilon^{u+1}}{(u+1)(1+\epsilon a)^{u+1}}\ (\gamma-a)^{u+1}$, is given by

$$\frac{-(1+\epsilon\ a)}{\epsilon} + a < \gamma < \frac{(1+\epsilon\ a)}{\epsilon} + a. \tag{34}$$

Appendix B
Meijer's G Function Expansion

The Meijer's G function can be expressed in terms of basic elementary functions. Applying the expansion in [20, eq. (9.303)] and $\lim_{z\to 0^+} {}_pF_q[e;f;z] = 1$, we have

$$G_{p,q}^{s,t}\left(z \mid \begin{matrix} c_1,\ldots,c_t,\ldots,c_p \\ d_1,\ldots,d_s,\ldots,d_q \end{matrix}\right) = \sum_{g=1}^{s} z^{d_g} \times \frac{\prod_{j=1;j\neq g}^{s} \Gamma\left(d_j - d_g\right) \prod_{j=1}^{t} \Gamma\left(1+d_g-c_j\right)}{\prod_{j=s+1}^{q} \Gamma\left(1+d_g-d_j\right) \prod_{j=t+1}^{p} \Gamma\left(c_j-d_g\right)}, \tag{35}$$

where $p \le q$, $|z| < 1$, and no two d_j (for $j = 1, 2, ..., t$) differ by an integer.

References

[1] I. Union, "IMT traffic estimates for the years 2020 to 2030," Int. Telecommun. Union, Geneva, Switzerland, Tech. Rep. ITU-R M. 2370–0, 2015.

[2] M. Giordani and M. Zorzi, "Non-terrestrial networks in the 6G era: Challenges and opportunities," *IEEE Network*, vol. 35, no. 2, pp. 244–251, 2020.

[3] S. C. Arum, D. Grace, and P. D. Mitchell, "A review of wireless communication using high-altitude platforms for extended coverage and capacity," *Computer Communications*, vol. 157, pp. 232–256, 2020.

[4] O. Kodheli, E. Lagunas, N. Maturo, S. K. Sharma, B. Shankar, J. F. M. Montoya, J. C. M. Duncan, D. Spano, S. Chatzinotas, S. Kisseleff, J. Querol, L. Lei, T. X. Vu, and G. Goussetis, "Satellite communications in the new space era: A survey and future challenges," *IEEE Communications Surveys & Tutorials*, vol. 23, no. 1, pp. 70–109, 2020.

[5] A. Dochhan, J. Poliak, J. Surof, M. Richerzhagen, H. F. Kelemu, and R. M. Calvo, "13.16 Tbit/s free-space optical transmission over 10.45 km for geostationary satellite feeder-links," in *Photonic Networks; 20th ITG-Symposium*, 2019, pp. 1–3.

[6] A. Trichili, M. A. Cox, B. S. Ooi, and M.-S. Alouini, "Roadmap to free space optics," *JOSA B*, vol. 37, no. 11, pp. A184–A201, 2020.

[7] M. Z. Chowdhury, M. K. Hasan, M. Shahjalal, M. T. Hossan, and Y. M. Jang, "Optical wireless hybrid networks: Trends, opportunities, challenges, and research directions," *IEEE Communications Surveys & Tutorials*, vol. 22, no. 2, pp. 930–966, 2020.

[8] S. Sharma, A. Madhukumar, and R. Swaminathan, "Capacity analysis for hybrid FSO/RF networks," *IEICE Proceedings Series*, vol. 55, no. We-AM-Poster. 11, 2018.

[9] N. Vishwakarma and R. Swaminathan, "Capacity analysis of adaptive combining for hybrid FSO/RF satellite communication system," in *2021 National Conference on Communications (NCC)*, 2021, pp. 1–6.

[10] N. D. Chatzidiamantis, G. K. Karagiannidis, E. E. Kriezis, and M. Matthaiou, "Diversity combining in hybrid RF/FSO systems with PSK modulation," in *2011 IEEE International Conference on Communications (ICC)*, 2011, pp. 1–6.

[11] R. Swaminathan, S. Sharma, N. Vishwakarma, and A. Madhukumar, "HAPS-based relaying for integrated space-air-ground networks with hybrid FSO/RF communication: A performance analysis," *IEEE Transactions on Aerospace and Electronic Systems*, vol. 57, no. 3, pp. 1581–1599, 2021.

[12] S. Shah, M. Siddharth, N. Vishwakarma, R. Swaminathan, and A. Madhukumar, "Adaptive-combining-based hybrid FSO/RF satellite communication with and without HAPS," *IEEE Access*, vol. 9, pp. 81 492–81 511, 2021.

[13] R. Samy, H.-C. Yang, T. Rakia, and M.-S. Alouini, "Performance analysis of hybrid SAG-FSO/RF satellite communication system," *TechRxiv. Preprint. https://doi.org/10.36227/techrxiv.19623849.v1*, 2022.

[14] T. V. Nguyen, H. D. Le, N. T. Dang, and A. T. Pham, "On the design of rate adaptation for relay-assisted satellite hybrid FSO/RF systems," *IEEE Photonics Journal*, vol. 14, no. 1, pp. 1–11, 2021.

[15] M. Usman, H.-C. Yang, and M.-S. Alouini, "Practical switching-based hybrid FSO/RF transmission and its performance analysis," *IEEE Photonics Journal*, vol. 6, no. 5, pp. 1–13, 2014.

[16] W. A. Alathwary and E. S. Altubaishi, "On the performance analysis of decode-and-forward multi-hop hybrid FSO/RF systems with hard-switching configuration," *IEEE Photonics Journal*, vol. 11, no. 6, pp. 1–12, 2019.

[17] R. Swaminathan, S. Sharma, and A. MadhuKumar, "Performance analysis of HAPS-based relaying for hybrid FSO/RF downlink satellite communication," in *2020 IEEE 91st Vehicular Technology Conference (VTC2020-Spring)*, 2020, pp. 1–5.

[18] H. Kaushal, V. Jain, and S. Kar, "Ground-to-satellite optical communication link performance with spatial diversity in weak atmospheric turbulence," *Fiber and Integrated Optics*, vol. 29, no. 4, pp. 315–340, 2010.

[19] I. S. Ansari, F. Yilmaz, and M.-S. Alouini, "Performance analysis of FSO links over unified Gamma-Gamma turbulence channels," in *2015 IEEE 81st Vehicular Technology Conference (VTC Spring)*, 2015, pp. 1–5.

[20] D. Zwillinger and A. Jeffrey, *Table of Integrals, Series, and Products*. Elsevier, 2007.

[21] A. Viswanath, V. K. Jain, and S. Kar, "Analysis of earth-to-satellite free-space optical link performance in the presence of turbulence, beam-wander induced pointing error and weather conditions for different intensity modulation schemes," *IET Communications*, vol. 9, no. 18, pp. 2253–2258, 2015.

[22] J. Ma, K. Li, L. Tan, S. Yu, and Y. Cao, "Performance analysis of satellite-to-ground downlink coherent optical communications with spatial diversity over Gamma–Gamma atmospheric turbulence," *Applied optics*, vol. 54, no. 25, pp. 7575–7585, 2015.

[23] E. Zedini, H. Soury, and M.-S. Alouini, "Dual-hop FSO transmission systems over Gamma–Gamma turbulence with pointing errors," *IEEE Transactions on Wireless Communications*, vol. 16, no. 2, pp. 784–796, 2016.

[24] M. K. Simon and M.-S. Alouini, *Digital Communication over Fading Channels*. John Wiley & Sons, 2005.

[25] G. Maral, M. Bousquet, and Z. Sun, *Satellite Communications Systems: Systems, Techniques and Technology*. John Wiley & Sons, 2020.

[26] "The wolfram research Meijer G-function document. acessed. July 25, 2022. [online]. available: https://functions.wolfram.com/pdf/meijerg.pdf."

[27] B. Kumbhani and R. Kshetrimayum, "Error performance of two-hop decode and forward relaying systems with source and relay transmit antenna selection," *Electronics Letters*, vol. 51, no. 6, pp. 530–532, 2015.

[28] T. Rakia, H.-C. Yang, M.-S. Alouini, and F. Gebali, "Outage analysis of practical FSO/RF hybrid system with adaptive combining," *IEEE Communications Letters*, vol. 19, no. 8, pp. 1366–1369, 2015.